

On the Invariants of Softmax Attention

Wonsuk Lee
Seoul National University & SK Hynix America
wonsuk.lee@snu.ac.kr

April 5, 2026

Abstract

Softmax attention maps every query–key interaction into a probability distribution, but the underlying structure remains largely unexplored. We define the *energy field*, the row-centered attention logit, and show that it exhibits invariant properties across models, architectures, and inputs.

Two classes of invariants emerge. *Mechanism-level* invariants follow from the algebraic structure of softmax attention. They include a per-row zero-sum constraint, a rank bound determined by the head dimension, and spectral signatures that follow from them. *Model-level* regularities are not required by the mechanism, yet hold in every autoregressive language model we test, spanning several architecture families. The energy field distributes its variance over key positions without concentrating at a few. This delocalization traces to a property of the key matrix we call *key incoherence*.

These invariants have practical consequences. The rank bound confines the energy field to a low-dimensional subspace. Key incoherence yields a per-head training monitor. All results are verified at multiple context lengths and input texts.

1 Introduction

The softmax attention mechanism [14] computes a compatibility score between every pair of query and key vectors, then normalizes these scores into a probability distribution that routes information between tokens. This mechanism is shared by all transformer language models, from GPT [11] to LLaMA [13] and Mistral [7].

Despite its engineering success, why dot-product softmax attention works so well in transformer language models is not understood. Theoretical work has studied expressiveness and approximation power [14], efficient alternatives [8, 5], and empirical patterns in the attention weights [15]. But what this simple mathematical structure produces when applied to language has not been characterized. Language has no known governing law or theory from which the effectiveness of attention can be derived. If structure exists in the attention computation, it must emerge from the interaction between the softmax mechanism and the data it processes. This paper searches for invariants of that interaction, as a step toward understanding what softmax attention computes beyond what it achieves.

To find these invariants, we define the *energy field* of a single attention head, the row-centered attention logit. It transforms the sparse, bounded attention probability p_{ij} into a representation that reveals what p_{ij} hides (Figure 1). Its properties divide into two categories.

Mechanism-level properties follow from softmax normalization and the bilinear form $Z_{ij} = q_i^\top k_j / \sqrt{d_h}$, where d_h is the head dimension. The row-sum identity ($\sum_j E_{ij} = 0$) produces an exact

autocovariance bridge in the flattened energy signal. The rank bound ($\leq d_h + 1$) confines the energy field to a low-dimensional subspace. Twenty SVD components capture over 90% of variance in the energy field at all context lengths tested.

Model-level regularities emerge from training on autoregressive language modeling. They are not required by the mechanism, yet they hold in every model we test. The central finding is *key incoherence*: the key norm concentration ratio μ_K stays near 1.5 in all 16 models spanning seven architecture families. There is no obvious reason for this agreement. The models differ in size, training data, and position encoding, but the regularity persists. It implies that the singular vectors of the energy field delocalize, and that the field concentrates its variance in far fewer dimensions than the rank bound allows.

Together, these properties characterize the intrinsic structure of softmax attention.

We verify all claims across 16 models spanning seven architecture families (124M–7B parameters), five context lengths ($L = 64$ to 1,024), and five input texts from Project Gutenberg, totaling 400 measurements. Every quantity is stable over input texts.

2 Related Work

Attention structure and patterns. Much prior work on the attention mechanism [14] focuses on the attention probability p_{ij} rather than the underlying logit structure. Xiao et al. [15] identified “attention sinks,” initial tokens that absorb disproportionate attention probability, and exploited them for efficient streaming inference. They did not formalize the structure behind them. The energy field (Definition 3.1) provides that structure. Attention sinks and other recurring patterns become measurable features of the energy field (Section 3).

Attention approximations. Linear attention [8] and the Performer [5] replace softmax with kernel-based approximations to reduce the quadratic cost of attention. These approximations break the exact row-sum cancellation that softmax enforces, a difference visible in the vanishing DC property (Section 7.1).

Matrix incoherence. The key incoherence parameter μ_K measures how uniformly the key norms spread across positions. The same quantity appears in matrix completion [4], where low-rank recovery requires the analogous condition $\mu = O(1)$. Our finding that trained transformers satisfy this condition connects softmax attention theory to a well-studied mathematical framework.

3 The Energy Field

3.1 Definitions

A single attention head [14] projects each token $x_i \in \mathbb{R}^{d_{\text{model}}}$ into a query $q_i = W_Q x_i$ and a key $k_j = W_K x_j$ in \mathbb{R}^{d_h} , where d_h is the head dimension. The attention logit $Z_{ij} = q_i^\top k_j / \sqrt{d_h}$ gives, in matrix form, $Z = QK^\top / \sqrt{d_h}$ with $Q, K \in \mathbb{R}^{L \times d_h}$. In autoregressive models, position i attends only to positions $j \leq i$, giving a causal context of size $n_i = i + 1$. The attention probability is $p_{ij} = \text{softmax}_j(Z_{ij}) = e^{Z_{ij}} / \sum_{j' \leq i} e^{Z_{ij'}}$, where j in softmax_j indicates normalization over key positions.

The attention probability p_{ij} is sparse, bounded, and entangled with a nonlinear partition function. The logit Z_{ij} is unbounded and linear but carries a position-dependent baseline. A query

with large norm produces high dot products with all keys, not just the relevant ones. This baseline skews the interaction pattern. Row centering removes it.

Definition 3.1 (Energy field). The *energy field* is the row-centered logit:

$$E_{ij} = Z_{ij} - \mu_i, \quad \mu_i = \frac{1}{n_i} \sum_{j'=0}^{n_i-1} Z_{ij'}, \quad (1)$$

where $n_i = i + 1$ is the causal context size at position i . By construction, $\sum_{j=0}^{n_i-1} E_{ij} = 0$ for every row i , the *row-sum identity*.

The transformation is invertible. Softmax is shift-invariant, so $p_{ij} = \text{softmax}_j(E_{ij})$. The energy field carries the information needed to compute the attention probability.

Remark 3.2 (Log-partition cancellation). Since $\log p_{ij} = Z_{ij} - \log Z_i$, the partition function cancels in mean centering, giving $E_{ij} = \log p_{ij} - (1/n_i) \sum_{j'} \log p_{ij'}$. The energy field is both a geometric quantity (centered dot products in embedding space) and a probabilistic one (mean-centered log-probability in attention space).

Definition 3.3 (Row-centered logit matrix). The *row-centered logit matrix* $\tilde{E} \in \mathbb{R}^{L \times L}$ is obtained by centering each row of the full logit matrix Z by its mean over all L key positions:

$$\tilde{E}_{ij} = Z_{ij} - \bar{\mu}_i, \quad \bar{\mu}_i = \frac{1}{L} \sum_{j'=0}^{L-1} Z_{ij'}. \quad (2)$$

By construction, $\sum_{j=0}^{L-1} \tilde{E}_{ij} = 0$ for every row i .

Remark 3.4 (Relationship between E and \tilde{E}). The causal energy field E_{ij} and the row-centered logit matrix \tilde{E}_{ij} start from the same logit Z_{ij} but subtract different row means. E_{ij} subtracts the causal mean $\mu_i = (1/n_i) \sum_{j'=0}^i Z_{ij'}$, the average over the $n_i = i + 1$ positions the model sees. \tilde{E}_{ij} subtracts the full mean $\bar{\mu}_i = (1/L) \sum_{j'=0}^{L-1} Z_{ij'}$, the average over all L positions.

The logit Z_{ij} is defined for all (i, j) pairs, including positions $j > i$ that the causal mask excludes during inference. \tilde{E}_{ij} therefore spans the full $L \times L$ matrix, while E_{ij} is defined only on the causal triangle ($j \leq i$). On that triangle, the two differ by a row-dependent constant $E_{ij} = \tilde{E}_{ij} + (\bar{\mu}_i - \mu_i)$, which shifts each row uniformly but does not affect within-row correlations or the rank structure.

The two objects serve different purposes. The causal energy field E_{ij} is the *physical* quantity that determines what softmax produces and drives the spectral signatures through the causal row-sum $\sum_{j=0}^i E_{ij} = 0$. The row-centered logit \tilde{E} is the *algebraic* tool, with clean properties that support the SVD decomposition and delocalization analysis.

3.2 Elementary properties

Two mechanism-level properties hold for any weights and any input. The **row-sum identity** $\sum_j E_{ij} = 0$ ensures that attention is a zero-sum competition among visible positions. Its spectral consequences are developed in Section 7.

The **rank bound** $\text{rank}(\tilde{E}) \leq d_h + 1$ follows because $Z = QK^T/\sqrt{d_h}$ has rank at most d_h , and row centering subtracts the rank-one matrix $\bar{\mu} \mathbf{1}^T$. By rank subadditivity, $\text{rank}(\tilde{E}) \leq d_h + 1$.

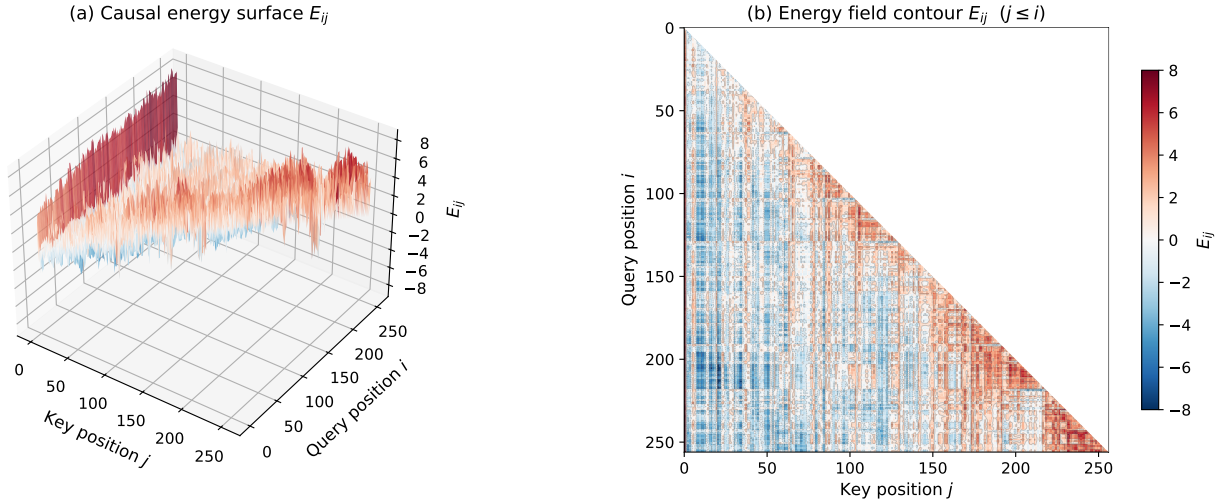


Figure 1: The causal energy field E_{ij} of a single LLaMA-3.2-1B head (layer 5, head 0, $L = 256$, processing Dickens). **(a)** Three-dimensional surface over the causal region ($j \leq i$). Ridges (red) mark high energy, valleys (blue) mark low energy. Every row sums to zero, so red and blue balance exactly. The acausal region ($j > i$) is masked. **(b)** Filled contour plot of the causal energy field, with iso-energy lines. Vertical stripes appear where key vectors produce consistently high or low energy for all queries. The triangular domain grows with i , reflecting the expanding causal context. Two features dominate. The diagonal ridge ($j = i$) carries mean energy $E_{ii} \approx 1.5$, reflecting self-attention since q_i and k_i project from the same embedding. The red band at $j = 0$ is far stronger, with mean $E_{i,0} \approx 6.1$. This is the BOS attention sink [15], visible as a column of uniformly high energy across all query positions.

3.3 A first look

Figure 1 shows E_{ij} for a single LLaMA-3.2-1B head at $L = 256$. The features are representative of all models tested (Sections 5–6). Two patterns dominate: the diagonal ridge ($E_{ii} \approx 1.5$, self-attention from shared embeddings) and the vertical band at $j = 0$ ($E_{i,0} \approx 6.1$, the attention sink [15]). Vertical stripes at other positions reflect key vectors that produce consistently high or low energy across all queries (Section 4).

3.4 The flattened signal

Definition 3.5 (Flattened signal). We construct the flattened signal by reading the causal energy field row by row, starting from row 1 (row 0 contains a single zero entry), to form a one-dimensional signal

$$\mathcal{E}_1, \mathcal{E}_2, \dots, \mathcal{E}_N, \quad N = \frac{L(L+1)}{2} - 1 \approx \frac{L^2}{2}. \quad (3)$$

Each position t maps to a unique row–column pair $(i(t), j(t))$, with $\mathcal{E}_t = E_{i(t), j(t)}$.

This ordering follows the causal structure of the attention mechanism. Consecutive entries within each row are nearby key positions, and row boundaries mark transitions to new queries. Since every row sums to zero, the global sum vanishes as $\sum_{t=1}^N \mathcal{E}_t = 0$. The spectral properties derived in Section 7 hold for any row-by-row ordering.

4 SVD Channel Decomposition

The rank bound gives at most $r \leq d_h + 1$ nonzero singular values. The SVD of \tilde{E} ,

$$\tilde{E} = \sum_{k=1}^r \sigma_k u_k v_k^T, \quad (4)$$

decomposes the energy field into r channels, where $u_k \in \mathbb{R}^L$ are query profiles and $v_k \in \mathbb{R}^L$ are key profiles.

On the causal triangle ($j \leq i$), the energy field E_{ij} differs from \tilde{E}_{ij} by the row-dependent constant $\bar{\mu}_i - \mu_i$ as in Remark 3.4, hence

$$E_{ij} = \sum_{k=1}^r \sigma_k (u_k)_i (v_k)_j + (\bar{\mu}_i - \mu_i), \quad j \leq i. \quad (5)$$

Each channel k pairs a query profile u_k with a key profile v_k . Within row i , the energy pattern is a weighted sum of key profiles with weights $\sigma_k \cdot (u_k)_i$. The key profiles are shared across all rows, producing the vertical stripes visible in Figure 1(b).

Rapid singular value decay. The rank bound is loose. The top 20 singular values of \tilde{E} capture 98% of total variance at $L = 256$ (Table 3), decreasing to 96% at $L = 512$ – $1,024$ as longer sequences contain richer structure within the subspace. Trained models concentrate variance in far fewer components than the mechanism allows.

Channel signals and autocovariance. The channel decomposition bounds the correlation structure of the flattened signal. This drives the spectral analysis of Section 7. To see how, we define the *per-channel signal* at position t using the flattened signal of Definition 3.5:

$$s_k(t) := \sigma_k \cdot (u_k)_{i(t)} \cdot (v_k)_{j(t)}, \quad (6)$$

then the full flattened signal is $\mathcal{E}_t = \sum_{k=1}^r s_k(t)$. The autocovariance of the flattened signal decomposes into channel cross-covariances:

$$\hat{\gamma}(\tau) = \frac{1}{N} \sum_{t=1}^{N-\tau} \mathcal{E}_t \mathcal{E}_{t+\tau} = \sum_{k=1}^r \sum_{l=1}^r \Gamma_{kl}(\tau), \quad (7)$$

where $\Gamma_{kl}(\tau) = (1/N) \sum_{t=1}^{N-\tau} s_k(t) s_l(t + \tau)$. There are at most $r^2 \leq (d_h + 1)^2$ such terms. A signal of length $N \approx L^2/2$ has its correlation structure captured by a fixed number of channel interactions determined by head dimension, not context length. This bounded complexity makes the autocovariance decomposition tractable.

5 Key Incoherence

The SVD of Section 4 decomposes the energy field into channels, but how are the singular vectors distributed spatially? Do they spread across all key positions, or concentrate at a few? The answer depends on the key matrix K .

Definition 5.1 (Key incoherence). For a key matrix $K \in \mathbb{R}^{L \times d_h}$ with rows k_0, \dots, k_{L-1} , the *key incoherence parameter* is

$$\mu_K = L \cdot \frac{\max_j \|k_j\|^2}{\|K\|_F^2}, \quad (8)$$

where $\|K\|_F^2 = \sum_{j=0}^{L-1} \|k_j\|^2$ is the squared Frobenius norm.

This parameter measures how uniformly the key norms are distributed across positions. When all keys have equal norm, $\mu_K = 1$. When a single key carries all the norm, $\mu_K = L$. For a random matrix with i.i.d. entries, $\mu_K \rightarrow 1$ as $L \rightarrow \infty$.

5.1 Main empirical result

Observation 5.2 (Key incoherence of trained language models). Across 5,888 key-value heads in 16 trained language models (124M–7B parameters), seven architecture families (Pythia, GPT-2, OPT, Qwen, LLaMA, Phi-2, Mistral), five context lengths ($L = 64$ –1,024), and five input texts from Project Gutenberg:

$$\mu_K = O(1). \quad (9)$$

Mean $\mu_K = 1.5$, maximum $\mu_K = 26$ (a single OPT-350m head). Excluding this outlier, the maximum is 8.6. The quantity is invariant across text genres with coefficient of variation below 3%.

Layer normalization controls $\|K\|_F^2/L$, keeping the average key norm at $O(d_h)$, but does not prevent $\max_j \|k_j\|^2$ from growing with L . A model that concentrates attention at a fixed position would have μ_K growing linearly with L . In practice, even randomly initialized models produce $\mu_K \approx 1.5$, because layer normalization equalizes $\|x_j\|$ over positions and random W_K introduces no positional bias. Training develops specialized attention patterns but preserves this uniformity. Table 1 confirms this for all seven architecture families.

Table 1: Key incoherence μ_K across architecture families (mean \pm std across all heads at $L = 256$).

Family	Models	Heads	μ_K (mean \pm std)	$\mu_K \leq 5$ (%)
Pythia	4	1,680	1.37 ± 0.4	100.0
GPT-2	3	1,248	1.74 ± 0.5	99.6
OPT	2	1,152	1.65 ± 0.7	99.1
Qwen	3	176	1.48 ± 0.2	100.0
LLaMA	2	352	1.49 ± 0.2	100.0
Phi-2	1	1,024	1.45 ± 0.3	99.9
Mistral	1	256	1.50 ± 0.2	100.0
All	16	5,888	1.5 ± 0.4	99.8

OPT-350m is the sole outlier, with a few heads reaching $\mu_K = 26$ at $L = 1,024$. OPT was released as a “warts and all” reproduction [17] with documented training instabilities. OPT-1.3B, from the same family, satisfies $\mu_K < 6$.

Remark 5.3. The row-sum identity and rank bound are mechanism-level, holding for any weights and any input. Key incoherence is empirical. Whether training on non-language tasks such as vision or protein modeling also preserves it remains open (Section 9).

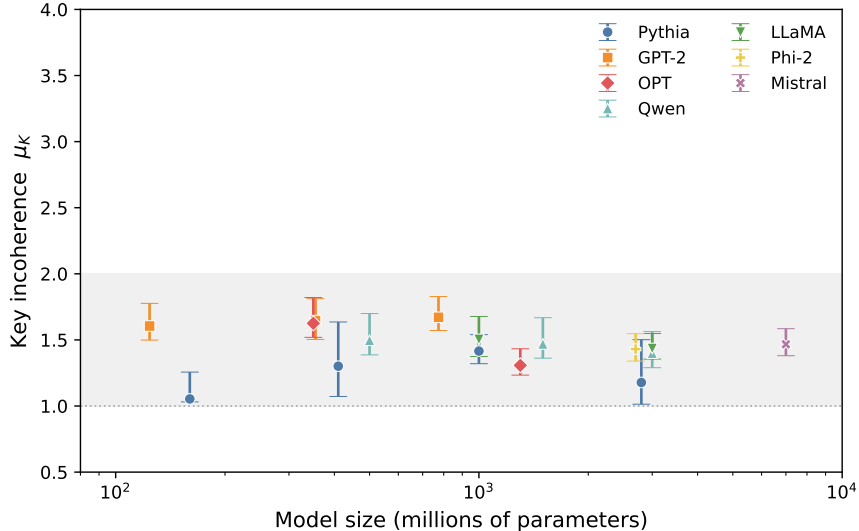


Figure 2: Key incoherence μ_K vs. model size for all 16 models at $L = 256$. Markers show the median μ_K across all heads; error bars span the interquartile range. Despite nearly two orders of magnitude in parameter count, μ_K shows no systematic trend and remains near 1.5 for every architecture family. The gray dotted line marks $\mu_K = 1$, perfectly uniform key norms.

5.2 Cross-architecture universality

Figure 2 plots μ_K against model size for all 16 models, spanning nearly two orders of magnitude in parameter count (124M to 7B). The key incoherence parameter shows no trend with model size, remaining near $\mu_K \approx 1.5$ from GPT-2 at 124M parameters to Mistral at 7B parameters. The interquartile ranges overlap for all architecture families. Neither the position encoding scheme, the training corpus, nor the model depth shifts μ_K appreciably.

6 Delocalization

With $\mu_K = O(1)$ established in Section 5, we can ask what it implies for the singular vectors of the energy field. They delocalize, spreading their mass across many positions rather than concentrating at a few. This section proves a bound on the delocalization and verifies it empirically.

Definition 6.1 (Inverse participation ratio). For a unit vector $v \in \mathbb{R}^L$, we define the *inverse participation ratio* as $\text{IPR}(v) = \sum_{j=0}^{L-1} v_j^4$.

The rescaled product $\text{IPR}(v) \cdot L$ is a dimensionless concentration index. It equals 1 for a perfectly uniform vector ($|v_j| = 1/\sqrt{L}$), L for a fully concentrated one ($v_1 = 1$ and the rest zero), and 3 for a Gaussian random vector ($v_j \sim \mathcal{N}(0, 1/L)$).

Lemma 6.2 (Delocalization bound). *Let $K \in \mathbb{R}^{L \times d_h}$ be the key matrix of an attention head, and let $\kappa(K) = \sigma_{\max}(K)/\sigma_{\min}(K)$ denote its condition number. Under the assumptions*

- (A-1) *Scale: $\|K\|_F^2/L = O(d_h)$ (automatic under layer normalization),*
- (A-2) *Incoherence: $\mu_K = O(1)$ (empirical; Section 5),*
- (A-3) *Conditioning: $\kappa(K)$ bounded independently of L (empirical; Remark 6.3 below),*

each right singular vector v_k of the row-centered logit matrix \tilde{E} satisfies

$$\text{IPR}(v_k) \cdot L \leq \frac{\mu_K \cdot d_h^2 \cdot \kappa^4}{L} \xrightarrow{L \rightarrow \infty} 0. \quad (10)$$

In particular, $\text{IPR}(v_k) \cdot L = O(1)$ for any fixed d_h .

Proof. The row space of $Z = QK^T/\sqrt{d_h}$ is a subspace of the column space of K , so the right singular vectors of Z lie in $\text{colspan}(K)$. Row centering adds a rank-one perturbation, so the right singular vectors of \tilde{E} lie in $\text{colspan}(K) + \text{span}(\mathbf{1})$. We prove the bound for any unit vector v in $\text{colspan}(K)$. The vector $\mathbf{1}/\sqrt{L}$ has $\text{IPR} = 1/L$, so $\text{IPR} \cdot L = 1$. It is maximally delocalized and satisfies the bound trivially.

Write $v = Kw/\|Kw\|$ for some $w \in \mathbb{R}^{d_h}$. Then $v_j = k_j^T w/\|Kw\|$, so by Cauchy–Schwarz:

$$v_j^2 \leq \frac{\|k_j\|^2 \|w\|^2}{\|Kw\|^2}.$$

Squaring both sides: $v_j^4 \leq \|k_j\|^4 \|w\|^4/\|Kw\|^4$. Summing over j and bounding each $\|k_j\|^2$ by $\max_j \|k_j\|^2$:

$$\text{IPR}(v) = \sum_j v_j^4 \leq \frac{\max_j \|k_j\|^2 \cdot \|K\|_F^2}{(\|Kw\|^2/\|w\|^2)^2}.$$

The denominator satisfies $\|Kw\|^2/\|w\|^2 \geq \sigma_{\min}^2(K)$, so $\text{IPR}(v) \leq \max_j \|k_j\|^2 \cdot \|K\|_F^2/\sigma_{\min}^4(K)$. Multiplying by L and using $\max_j \|k_j\|^2 = \mu_K \|K\|_F^2/L$ (Definition 5.1):

$$\text{IPR}(v) \cdot L \leq \mu_K \cdot \frac{\|K\|_F^4}{L \cdot \sigma_{\min}^4(K)}.$$

(A-1) ensures $\|K\|_F^2 = O(L d_h)$, keeping the bound finite. SVD of K gives $\|K\|_F^2 = \sum_{k=1}^{d_h} \sigma_k^2(K)$. With (A-3), we get $\sigma_{\min}^2(K) \geq \|K\|_F^2/(d_h \kappa^2)$, so $\sigma_{\min}^4(K) \geq \|K\|_F^4/(d_h^2 \kappa^4)$. Substituting:

$$\text{IPR}(v) \cdot L \leq \mu_K \cdot \frac{\|K\|_F^4}{L \cdot \|K\|_F^4/(d_h^2 \kappa^4)} = \frac{\mu_K \cdot d_h^2 \cdot \kappa^4}{L}. \quad \square$$

Remark 6.3 (Conditioning assumption). (A-3) requires that K uses all d_h dimensions of the key space, so that $\sigma_{\min}(K) > 0$. Empirically, the median $\kappa(K)$ ranges from 20 to 570 at $L = 256$ – $1,024$ and *decreases* with context length. For example, GPT-2 has median $\kappa = 49$ at $L = 256$ and 24 at $L = 1,024$. At short contexts ($L < d_h$), the key matrix is rank-deficient and κ is unbounded. The condition number is not $O(1)$ in the strict sense, but it does not grow with L , which is what the bound requires. A well-trained model uses all dimensions of its key space. Gradients repurpose any that carry no information.

Key incoherence and bounded conditioning together force $\text{IPR}(v_k) \cdot L \rightarrow 0$. We verify this in 16 models at five context lengths and five texts (Table 2). In all 400 measurements, $\text{IPR} \cdot L$ ranges from 2.85 to 3.63, close to the Gaussian random vector baseline of 3. Within each model, the cross-text CV is below 2%.

Non-RoPE architectures (GPT-2, OPT) cluster near $\text{IPR} \cdot L \approx 3.4$, while RoPE-based families cluster near 3.0. Rotary embeddings [12] spread key vectors more uniformly on the d_h -dimensional sphere, producing slightly more delocalized singular vectors. The value decreases with context length, from 3.27 at $L = 64$ to 3.04 at $L = 1,024$, consistent with the bound.

Table 2: Delocalization ($\text{IPR} \cdot L$) of \tilde{E} at $L = 512$. RoPE-based architectures show systematically lower values than non-RoPE models.

Family	Models	IPR $\cdot L$ (mean)	CV (%)
GPT-2	3	3.46 ± 0.15	4.2
OPT	2	3.42 ± 0.10	2.8
Pythia	4	3.05 ± 0.08	2.7
Qwen	3	2.95 ± 0.04	1.3
LLaMA	2	3.10 ± 0.07	2.2
Phi-2	1	3.04	—
Mistral	1	3.25	—
All (16 models)	16	3.17 ± 0.21	6.7

7 Spectral Signatures

The row-sum identity constrains the spectral structure of the flattened signal \mathcal{E}_t (Definition 3.5). Correlations between energy values at different positions and scales are invisible in the matrix but exposed by spectral decomposition. The row-sum produces an exact autocovariance bridge when squared. The DC component also vanishes, a direct consequence of the zero mean. Both properties are mechanism-level and hold for any model. We verify them using the discrete wavelet transform to analyze the non-stationary flattened signal.

7.1 The discrete wavelet transform

The flattened signal concatenates rows of increasing length and is non-stationary by construction. We use the discrete wavelet transform [10] (DWT) with a Daubechies-4 wavelet in periodization mode, which handles non-stationarity and conserves energy exactly (Parseval’s theorem):

$$\sum_t \mathcal{E}_t^2 = \sum_n a_J[n]^2 + \sum_{j=1}^J \sum_n d_j[n]^2, \quad (11)$$

where $a_J[n]$ are approximation coefficients at the coarsest level and $d_j[n]$ are detail coefficients at scale 2^j . The *approximation fraction* $\rho = \sum_n a_J[n]^2 / \sum_t \mathcal{E}_t^2$ measures the DC content, and the *wavelet energy density* $\mathcal{W}(j) = (1/N_j) \sum_n d_j[n]^2$ characterizes the multi-scale correlation structure. The flattened signal has zero mean by construction. The wavelet approximation fraction $\rho < 0.004$ in all 400 measurements confirms this (Figure 3(a)).

7.2 The autocovariance bridge

The flattened signal pairs entries from the same row, called *within-row*, or from different rows, called *cross-row*. For each row i , the *per-row autocovariance* is $S_i(\tau) = \sum_{j=0}^{n_i-1-\tau} E_{ij} E_{i,j+\tau}$. The *within-row autocovariance* is $W(\tau) = \sum_i S_i(\tau)$, summed over rows with $n_i > \tau$, and the *cross-row autocovariance* is the remainder $X(\tau) = N\hat{\gamma}(\tau) - W(\tau)$.

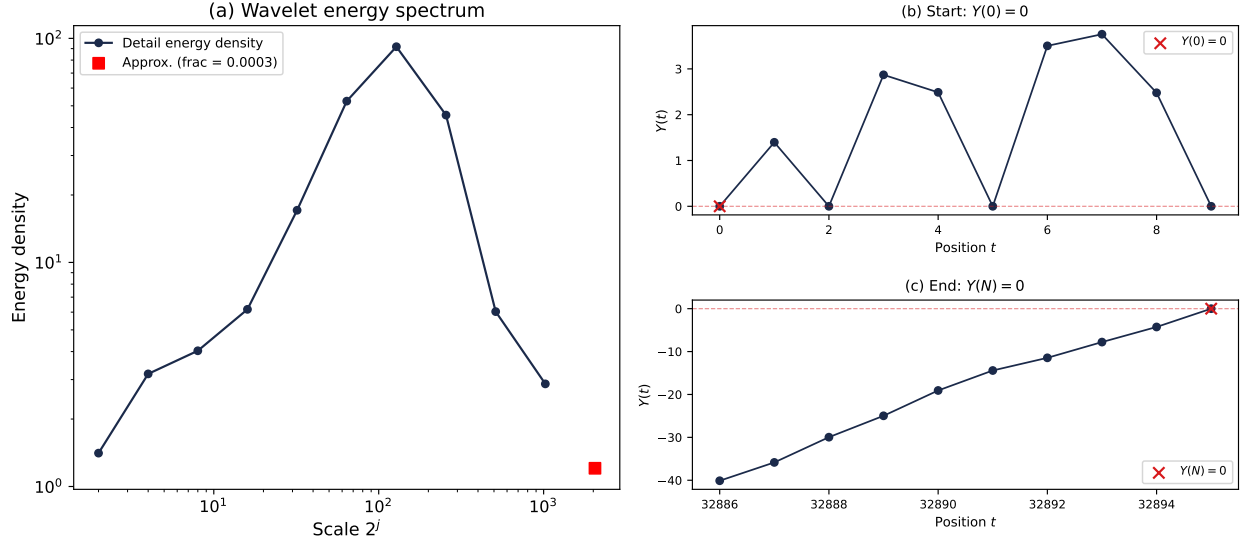


Figure 3: Spectral signatures in the flattened energy signal of LLaMA-3.2-1B, layer 5, head 0, $L = 256$. **(a)** Wavelet energy spectrum. Energy density increases with scale in the detail subbands. The coarsest approximation (red square) carries < 0.004 of total energy, verifying the vanishing DC property. **(b, c)** First and last 10 values of the cumulative signal $Y(t) = \sum_{s=1}^t \mathcal{E}_s$. The signal starts at $Y(0) = 0$ and returns to $Y(N) = 0$, a bridge pinned at both ends. This is a direct consequence of the row-sum identity $\sum_t \mathcal{E}_t = 0$.

Proposition 7.1 (Bridge identity). *The row-sum identity implies*

$$\sum_{\tau \geq 0} W(\tau) = \frac{N\hat{\gamma}(0)}{2}, \quad \sum_{\tau=0}^{N-1} \hat{\gamma}(\tau) = \frac{\hat{\gamma}(0)}{2}. \quad (12)$$

Proof. For row i with n_i entries, the row-sum constraint gives $\sum_{j=0}^{n_i-1} E_{ij} = 0$. Squaring both sides,

$$0 = \left(\sum_{j=0}^{n_i-1} E_{ij} \right)^2 = \sum_j \sum_{j'} E_{ij} E_{ij'}.$$

Grouping the double sum by lag $\tau = j' - j$, the $\tau = 0$ terms give $\sum_j E_{ij}^2 = S_i(0)$, and each nonzero lag τ appears twice (once for $j' - j = \tau$, once for $j - j' = \tau$), giving

$$S_i(0) + 2 \sum_{\tau=1}^{n_i-1} S_i(\tau) = 0.$$

Summing over all rows i ,

$$W(0) + 2 \sum_{\tau \geq 1} W(\tau) = 0.$$

Since $W(0) = \sum_i S_i(0) = \sum_t \mathcal{E}_t^2 = N\hat{\gamma}(0)$, rearranging gives the first identity $\sum_{\tau \geq 0} W(\tau) = N\hat{\gamma}(0)/2$.

For the second identity, apply the same argument to the global sum $\sum_{t=1}^N \mathcal{E}_t = 0$. Squaring,

$$0 = \sum_{t=1}^N \sum_{t'=1}^N \mathcal{E}_t \mathcal{E}_{t'}.$$

Grouping by lag $\tau = t' - t$ and using symmetry $\hat{\gamma}(-\tau) = \hat{\gamma}(\tau)$,

$$0 = N\hat{\gamma}(0) + 2 \sum_{\tau=1}^{N-1} N\hat{\gamma}(\tau).$$

Dividing by N gives $\hat{\gamma}(0) + 2 \sum_{\tau=1}^{N-1} \hat{\gamma}(\tau) = 0$, hence $\sum_{\tau=1}^{N-1} \hat{\gamma}(\tau) = -\hat{\gamma}(0)/2$. Adding $\hat{\gamma}(0)$ to include the $\tau = 0$ term, $\sum_{\tau=0}^{N-1} \hat{\gamma}(\tau) = \hat{\gamma}(0)/2$. \square

The cumulative signal $Y(t) = \sum_{s=1}^t \mathcal{E}_s$ starts at zero and returns to zero, a *bridge* pinned at both ends (Figure 3(b, c)). We verify the bridge ratio $\sum W(\tau)/[N\hat{\gamma}(0)/2] = 1.000000$ to six decimal places in all 400 measurements.

The bridge identity means that within-row correlations account for exactly half the total energy, and cross-row correlations account for the other half. This even split holds regardless of the model, the input, or the context length. It is a structural constraint on how attention organizes information, imposed by the row-sum identity alone.

This analysis is tractable because the autocovariance decomposes into at most $r^2 \leq (d_h + 1)^2$ channel interactions (Eq. (7)), a bound determined by head dimension, not context length. The wavelet transform reveals the multi-scale correlation structure and verifies the bridge identity.

8 Implications

8.1 Intrinsic dimensionality of the energy field

The rank bound ($\text{rank}(\tilde{E}) \leq d_h + 1$) establishes that the energy field lives in a low-dimensional subspace. Trained models use far less of this subspace than the bound allows.

The reconstruction fidelity $F_r = 1 - \|M - M_r\|_F^2 / \|M\|_F^2$ measures the fraction of total variance captured by a rank- r approximation. Table 3 compares SVD on the row-centered logit matrix \tilde{E} and the causal field E against a top- k sparsification baseline that keeps the k largest entries per row.

Table 3: Reconstruction fidelity F_r for three methods (mean across GPT-2, Pythia-410M, LLaMA-3.2-1B at $L = 256$). SVD dominates at every rank, confirming that the energy field is low-rank, not sparse.

r	SVD(\tilde{E})	SVD(E)	Top- k
5	0.89	0.76	0.25
10	0.94	0.85	0.38
20	0.98	0.92	0.54

At $r = 20$, SVD on \tilde{E} captures 98% of variance while top- k captures only 54%. The energy field is low-rank, not sparse. SVD on \tilde{E} outperforms SVD on E because the rank bound applies to \tilde{E} directly. The causal field E differs by row-dependent shifts (Remark 3.4), which spread variance beyond the rank-bounded subspace.

The intrinsic dimensionality of the energy field is ~ 20 out of the $d_h + 1 = 65$ dimensions the rank bound allows. Trained models concentrate their attention structure in far fewer components than the mechanism permits. Whether this low-rank structure can be exploited at inference time is open, because softmax amplifies reconstruction errors at peak-attention positions. A companion paper [9] proves that the attention error under rank- r truncation is bounded by the delocalization constant and the tail singular values, providing a first bridge between the structural findings here and inference-time fidelity.

8.2 μ_K as a training monitor

A head with $\mu_K \gg 1$ concentrates its key norms at one or a few positions, collapsing attention toward fixed targets. Monitoring μ_K during training can detect this pathology early.

The computation is negligible. At each logging step, for each head, compute $\mu_K = L \cdot \max_j \|k_j\|^2 / \sum_j \|k_j\|^2$ from the key vectors. The additional cost is one `max` and one `sum`.

For 5,888 heads in 16 models, 99.8% have $\mu_K \leq 5$ (Table 1). We suggest $\mu_K = 5$ as a warning threshold. The threshold is derived from post-hoc analysis of trained models. Validating it as a live training monitor remains future work.

9 Discussion

9.1 Experimental scope and limitations

We test 16 models from seven architecture families: Pythia [3] (160M, 410M, 1B, 2.8B), GPT-2 [11] (124M, 355M, 774M), OPT [17] (350M, 1.3B), Qwen-2.5 [16] (0.5B, 1.5B, 3B), LLaMA-3.2 [13] (1B, 3B), Phi-2 [6] (2.7B), and Mistral-7B [7] (7B). Five of the seven families use rotary position embeddings (RoPE) [12] and three use grouped query attention (GQA) [1], where fewer key-value heads serve multiple query heads. Models up to 3B run in float32; Mistral-7B runs in float16.

Input texts are five excerpts ($\sim 3,000$ words each) from Project Gutenberg: Dickens (*A Tale of Two Cities*), Darwin (*On the Origin of Species*), Shakespeare (*Hamlet*), the King James Bible, and Adam Smith (*The Wealth of Nations*). The DWT pipeline is validated against synthetic ground-truth tests, including Parseval conservation to machine precision. All reported quantities have CV $< 10\%$ over the five texts, with $\text{IPR} \cdot L$ below 2% within each model.

The scope has clear boundaries. All models are autoregressive language models trained on English-dominant corpora. The largest model (Mistral, 7B) is small by current standards; models at 70B and above may exhibit different conditioning or attention specialization. Context lengths reach $L = 1,024$, well below the 32K–128K windows of modern long-context models. The mechanism-level results (row-sum, rank bound, bridge identity) hold by construction and are not affected by these limitations. The model-level results ($\mu_K = O(1)$, delocalization) are empirical claims whose generality depends on the breadth of models tested.

9.2 Open problems

The connection between μ_K and the coherence parameter in matrix completion [4], noted in Section 2, suggests that tools from random matrix theory may apply to the energy field.

1. *Why does training preserve $\mu_K = O(1)$?* Random initialization establishes incoherence. Training develops specialized attention patterns while maintaining it. Deriving this preservation from gradient descent dynamics would unify the mechanism-level and model-level results.

2. *Can the delocalization bound be tightened?* The current bound establishes the correct asymptotic behavior ($\text{IPR} \cdot L \rightarrow 0$) but is quantitatively loose. A tighter analysis exploiting the full spectrum of K would narrow the gap between the bound and the empirical range of 2.85–3.63.
3. *Does $\mu_K = O(1)$ hold beyond language?* Scaling to 70B+ models, testing at $L = 32\text{K}–128\text{K}$, and measuring μ_K on vision transformers, protein models, and reinforcement learning agents would determine whether key incoherence is specific to natural language or general to softmax attention.
4. *Can the low intrinsic dimensionality be exploited?* The energy field concentrates most of its variance in far fewer than $d_h + 1$ components, but the softmax nonlinearity amplifies reconstruction errors at peak-attention positions. Bridging this gap requires methods that account for the interaction between low-rank approximation and softmax.

10 Conclusion

The energy field $E_{ij} = Z_{ij} - \mu_i$ is a complete, invertible representation of softmax attention. Two algebraic constraints govern it. Each row sums to zero, and the matrix has rank at most $d_h + 1$.

The central finding is key incoherence. Every trained language model we test maintains $\mu_K \approx 1.5$, keeping key norms spread over positions despite developing specialized attention patterns. This regularity holds in 16 models spanning seven architecture families, from 124M to 7B parameters. It implies that the singular vectors of the energy field delocalize, and that the field concentrates its variance in far fewer components than the mechanism allows.

The energy field is more structured than the mechanism requires and more uniform than one might expect. Understanding why training preserves this uniformity remains open.

References

- [1] Joshua Ainslie, James Lee-Thorp, Michiel de Jong, Yury Zemlyanskiy, Federico Lebrón, and Sumit Sanghai. GQA: Training generalized multi-query transformer models from multi-head checkpoints. In *Proceedings of EMNLP*, 2023.
- [2] John Aitchison. *The Statistical Analysis of Compositional Data*. Chapman & Hall, 1986.
- [3] Stella Biderman, Hailey Schoelkopf, Quentin Gregory Anthony, Herbie Bradley, Kyle O’Brien, Eric Hallahan, Mohammad Aflah Khan, Shivanshu Purohit, USVSN Sai Prashanth, Edward Raff, et al. Pythia: A suite for analyzing large language models across training and scaling. In *International Conference on Machine Learning*, 2023.
- [4] Emmanuel J Candès and Benjamin Recht. Exact matrix completion via convex optimization. *Foundations of Computational Mathematics*, 9(6):717–772, 2009.
- [5] Krzysztof Marcin Choromanski, Valerii Likhoshesterov, David Dohan, Xingyou Song, Andreea Gane, Tamas Sarlos, Peter Hawkins, Jared Quincy Davis, Afroz Mohiuddin, Lukasz Kaiser, et al. Rethinking attention with performers. In *International Conference on Learning Representations*, 2021.
- [6] Mojan Javaheripi et al. Phi-2: The surprising power of small language models. *Microsoft Research Blog*, 2023.

- [7] Albert Q Jiang, Alexandre Sablayrolles, Arthur Mensch, Chris Bamford, Devendra Singh Chaplot, Diego de las Casas, et al. Mistral 7B. *arXiv preprint arXiv:2310.06825*, 2023.
- [8] Angelos Katharopoulos, Apoorv Vyas, Nikolaos Pappas, and François Fleuret. Transformers are RNNs: Fast autoregressive transformers with linear attention. In *International Conference on Machine Learning*, 2020.
- [9] Wonsuk Lee. Compressible softmax-attended language under incompressible attention. *arXiv preprint*, 2026.
- [10] Stéphane Mallat. *A Wavelet Tour of Signal Processing: The Sparse Way*. Academic Press, 3rd edition, 2009.
- [11] Alec Radford, Jeffrey Wu, Rewon Child, David Luan, Dario Amodei, and Ilya Sutskever. Language models are unsupervised multitask learners. *OpenAI Technical Report*, 2019.
- [12] Jianlin Su, Murtadha Ahmed, Yu Lu, Shengfeng Pan, Wen Bo, and Yunfeng Liu. RoFormer: Enhanced transformer with rotary position embedding. *Neurocomputing*, 568:127063, 2024.
- [13] Hugo Touvron, Thibaut Lavril, Gautier Izacard, Xavier Martinet, Marie-Anne Lachaux, Timothée Lacroix, Baptiste Rozière, Naman Goyal, Eric Hambro, Faisal Azhar, et al. LLaMA: Open and efficient foundation language models. *arXiv preprint arXiv:2302.13971*, 2023.
- [14] Ashish Vaswani, Noam Shazeer, Niki Parmar, Jakob Uszkoreit, Llion Jones, Aidan N Gomez, Łukasz Kaiser, and Illia Polosukhin. Attention is all you need. In *Advances in Neural Information Processing Systems*, volume 30, 2017.
- [15] Guangxuan Xiao, Yuandong Tian, Beidi Chen, Song Han, and Mike Lewis. Efficient streaming language models with attention sinks. In *International Conference on Learning Representations*, 2024.
- [16] An Yang, Baosong Yang, Binyuan Hui, Bo Zheng, Bowen Yu, Chang Zhou, et al. Qwen2 technical report. *arXiv preprint arXiv:2407.10671*, 2024.
- [17] Susan Zhang, Stephen Roller, Naman Goyal, Mikel Artetxe, Moya Chen, Shuohui Chen, Christopher Dewan, Mona Diab, Xian Li, Xi Victoria Lin, et al. OPT: Open pre-trained transformer language models. *arXiv preprint arXiv:2205.01068*, 2022.

A Appendix: The energy field as a centered log-ratio transform

The arithmetic mean used to define the energy field (Definition 3.1) is the unique centering that corresponds to the geometric mean of the attention probabilities, the natural center of a distribution on the probability simplex.

The geometric mean of the attention probabilities in row i is $\bar{p}_i^{(G)} = (\prod_{j'} p_{ij'})^{1/L}$. Since $\log p_{ij} = Z_{ij} - \log \mathcal{Z}_i$, the log-geometric-mean is

$$\log \bar{p}_i^{(G)} = \frac{1}{L} \sum_{j'} \log p_{ij'} = \frac{1}{L} \sum_{j'} Z_{ij'} - \log \mathcal{Z}_i = \bar{\mu}_i - \log \mathcal{Z}_i.$$

The log-ratio of each probability to this geometric mean is

$$\log \frac{p_{ij}}{\bar{p}_i^{(G)}} = (Z_{ij} - \log \mathcal{Z}_i) - (\bar{\mu}_i - \log \mathcal{Z}_i) = Z_{ij} - \bar{\mu}_i = \tilde{E}_{ij}.$$

The partition function Z_i cancels exactly. The energy field is the log-ratio of each attention probability to the geometric mean of its row. Positive energy means a position receives more attention than the geometric average. The geometric mean, not the arithmetic mean, is the correct reference because softmax maps logits through an exponential.

This is the *centered log-ratio* (CLR) transform from compositional data analysis [2]. Attention probabilities are compositions. They are nonnegative and sum to one. The CLR transform maps the probability simplex to \mathbb{R}^L with two properties. First, the components sum to zero (the row-sum identity of Definition 3.1). Second, the Euclidean inner product in CLR coordinates equals the Aitchison inner product on the simplex, the natural metric for compositional data.

By the Eckart–Young theorem, SVD minimizes the Frobenius-norm reconstruction error at any rank. Since the Frobenius norm in CLR coordinates equals the Aitchison distance on the simplex, the SVD of the energy field (Section 4) gives the optimal low-rank approximation of the attention pattern in the Aitchison geometry, not merely in Euclidean distance. The rank bound, key incoherence, and delocalization results all hold in the coordinate system that respects the compositional structure of attention.

Alternative centerings fail. Any nonlinear function of the logits breaks the row-sum identity $\sum_j (Z_{ij} - \bar{Z}_i) = 0$, which underpins the spectral results. Any centering of the probabilities other than the geometric mean fails to cancel the partition function. The arithmetic mean of logits is the only centering that is both linear in Z and meaningful on the probability simplex.

The arithmetic mean of logits is the unique centering that is both linear in Z (preserving the algebraic structure) and equivalent to the geometric mean of probabilities (respecting the compositional geometry of the simplex).